

Article

Synergy between Ionic Liquids and CuCl₂ in Gas–Liquid Phase Reactions of Acetylene Hydrochlorination

Yi Yu ^{1,2}, Yuxue Yue ¹, Bolin Wang ¹, Haihua He ¹, Zhong-Ting Hu ³, Jia Zhao ^{1,*} and Xiaonian Li ^{1,*}¹ Industrial Catalysis Institute, Laboratory Breeding Base of Green Chemistry-Synthesis Technology, Zhejiang University of Technology, Hangzhou 310014, China; yiyu@zjut.edu.cn (Y.Y.); yueyuxue152851@163.com (Y.Y.); wbl501028@outlook.com (B.W.); hehaihua2002@jhc.edu.cn (H.H.)² College of Chemical Engineering, Zhejiang University of Technology, Hangzhou 310014, China³ College of Environment, Zhejiang University of Technology, Hangzhou 310014, China; zthu@zjut.edu.cn

* Correspondence: jiazhao@zjut.edu.cn (J.Z.); xnli@zjut.edu.cn (X.L.); Tel.: +86-571-88871565 (J.Z.); +86-571-88320002 (X.L.)

Received: 9 May 2019; Accepted: 30 May 2019; Published: 31 May 2019



Abstract: We studied the acetylene hydrochlorination in gas–liquid phase reactions using ionic liquids (IL) as the reaction media and CuCl₂ as the catalyst. The Cu-IL catalyst showed strong synergy between the IL and the Cu(II) active catalytic species. For [PrMIm]Cl, the Cu-IL catalyst exhibited significant enhancement of the catalytic activity in comparison with the CuCl₂ catalyst supported on activated carbon and the IL alone as the catalyst. We have also performed DFT calculations of the reaction process, which provides a good explanation of our experimental results and for the synergistic effect. Our result suggests that ILs may be used to improve the activity of other metallic catalysts for the hydrochlorination reaction of acetylene.

Keywords: ionic liquids; CuCl₂ catalyst; acetylene hydrochlorination; synergistic effect

1. Introduction

The conventional catalyst HgCl₂ for acetylene hydrochlorination in the PVC industry has to be replaced by mercury-free catalysts worldwide due to its pollution to the environment. Early in 1984, Hutchings uncovered a correlation between the standard electrode potential of various metals and their catalytic activity, and proposed that gold is a highly active catalyst for acetylene hydrochlorination [1]. Since then, a lot of focus has been concentrated on noble metals including Au, Pt, and Pd as catalysts for their high standard electrode potentials [2–4]. However, these noble metal based catalysts are very costly, and still suffer from issues of loss of activity [5]. In recent years, searching for alternative non-noble metal catalysts with low costs while still maintaining high catalytic activity has attracted a lot of interest and taken a lot of research effort.

Among the non-noble metal catalysts that have been studied in the literature are Cu, Sn, Mn, Zn, Co, and Bi [6–11]. These metals often have relatively lower standard electrode potentials when compared with noble metals. Therefore, a mono-metallic catalyst of these metals usually does not have very high catalytic activity. In order to improve the catalytic activity, bimetallic and trimetallic catalysts have been prepared and investigated in the literature [11–13] in the hope that the synergy between multicomponents of metals may lead to much enhanced activity. The non-noble metals may act as an assistive to a noble metal catalyst, or they can cooperate with other non-noble metals to form bimetallic or trimetallic catalysts [14,15].

Recently, the extraordinary properties of ionic liquids (ILs), such as low vapor pressure and high salvation strength, have caught a lot of attention [16–18]. There have been many reports of significant

promotion of catalytic activity by ILs [18]. Furthermore, ILs alone have been used as a mercury-free catalyst as well. Cao and coworkers [19] studied the influence of some ionic liquids on the performance of mercury-free catalysts and found that [BMIm]Cl could increase the acetylene conversion rate up to 68%. In addition, they also studied its effect on the performance of other metal chlorides that act as the main active species of the catalysts. Except for SnCl₄, they found significant enhancement of the acetylene conversion rate for HgCl₂, MnCl₄, H₂[PtCl₆], and H[AuCl₄]. Zhao et al. prepared supported IL phase (SILP) stabilized Au(III) catalyst for acetylene hydrochlorination, without [20] and with [21] the additive of CuCl₂, and reported an outstanding catalytic performance. Zhang et al. [22] recently reported that the imidazolium type of IL, [BMIm]BF₄, may substantially increase the performance of a Ru catalyst supported on activated carbon (AC), despite it being not a good catalyst on its own. Lately, Cao et al. [23] investigated the performance of imidazolium ILs as mercury-free catalysts for acetylene hydrochlorination. They found that [BMIm]Cl exhibited good catalytic performance. Strong promotional effect of ILs on Pd catalyst using the SILP technique has also been reported lately [24]. Thus far, existing research demonstrates that ILs may promote the performance of a catalyst. Nonetheless, there are still no systematic study of such enhancement effect, such as extent of the enhancement, decisive factors, and underlying mechanism. For example, Cao et al. [19] did not provide comparison against the performance of the metal chloride catalysts under the same preparation and reaction conditions but without the ILs.

On the other hand, studies reveal that nitrogen doping to the activated carbon support may significantly enhance the catalytic activity [25–28]. This has been attributed to the modification effect of the nitrogen-containing species to the surface chemistry of the AC support. It also demonstrates that these nitrogen-containing species may serve as active sites for catalytic reactions [29–32]. Based on these studies, here we chose imidazolium based ILs, which contain two N atoms per molecule, as our main reaction media. At the same time, we prepared the catalyst by adding non-noble metal chlorides, including CuCl₂, FeCl₃, SnCl₂, ZnCl₂, BiCl₂, and BiCl₃. These metal chlorides have been studied as an additive in preparing bimetallic catalysts with Au (or Pt and Pd), which may possess higher activity than the mono-metallic Au catalyst [7,15]. Our result showed that CuCl₂ has the best catalytic performance. When combined with ILs, CuCl₂ and the N sites of the imidazolium ring act together to increase the adsorption of HCl and C₂H₂, and thus facilitate the hydrochlorination reaction of acetylene. In this paper, we will focus our study on the synergetic effect of ILs and metals, and find out the best combination as a catalyst for acetylene hydrochlorination, and try to reveal the underlying mechanism.

Our experimental result demonstrates that [PrMIm]Cl and CuCl₂ can cooperate and exhibit a good synergy in catalyzing acetylene hydrochlorination reactions. The synergetic catalyst exhibits much better performance than the CuCl₂/AC catalyst and [PrMIm]Cl alone as a catalyst. To understand this result, we have performed a mechanistic study using DFT calculations.

The authors of [23] proposed a model for the reaction process of [BMIm]Cl alone as a mercury-free catalyst for acetylene hydrochlorination. However, there have been no calculations for [PrMIm]Cl as a catalyst, nor for the catalyst CuCl₂-[PrMIm]Cl. For this reason, we have performed quantum chemistry calculations using the DFT theory. Our calculations provide a good explanation for our experimental result and the synergy between the IL and CuCl₂.

2. Results

In this section, we will first present the result of the evaluation experiments, followed by characterizations of the catalysts. Then we will show our result of DFT calculations, to reveal a mechanism for the enhancement effect of the ILs.

2.1. Experimental Results

We analyzed the thermal stability of the ILs using thermal gravimetric analysis (TGA). The TGA curves for [PrMIm]Cl and [BMIm]Cl are shown in Supplementary Figure S1. The thermal decomposition products were determined by infrared FT-IR measurements. The FT-IR data indicate that the onset of

mass loss is about 195 °C and 150 °C for [BMIm]Cl and [PrMIm]Cl, respectively, far below the thermal decomposition temperature T_d . Therefore, for [BMIm]Cl and [PrMIm]Cl, the ideal reaction temperature should be kept below 195 °C and 150 °C, respectively, in order to maintain long term stability.

The TGA result for other ILs in our experiments was similar, with rapid thermal decomposition occurring around the thermal decomposition temperature T_d (see Table 2 below in the Materials section). As for the small amount of decomposition products, there are thus far no conclusive data to tell whether such decomposition will continue or stop at this temperature. The TGA analysis cannot provide such information, since the temperature was raised typically at a rate of 10 °C /min, and thus only provides short-term data.

Shown in Figure 1 are the FT-IR spectra of (a) the IL [PrMIm]Cl and (b) the catalyst [PrMIm]Cl-CuCl₂, respectively. The broad peak around 3400 cm⁻¹ was from the stretching modes of various O–H bonds from water contamination. The band around 3000 cm⁻¹ mainly came from the C–H bonding in the IL. In addition, there should also be broad vibrational modes associated the N–H bonds around 3200 cm⁻¹ [33]. In comparison, we find that the absorption peak at 1458.6 cm⁻¹ was shifted up to 1462.7 cm⁻¹, and the peak at 3073.3 cm⁻¹ was shifted to 3076.5 cm⁻¹, while the peak at 1636.3 cm⁻¹ was shifted down to 1634.4 cm⁻¹. Shown in Figure 2 is the calculated adsorption structure of [CuCl₄]²⁻ on the cation [PrMIm]⁺. Based on this structure, we calculated the IR absorption spectrum. After careful comparison and review of the animation for the vibration modes of the calculated spectrum, we found that the 1458.6 cm⁻¹ and 1462.7 cm⁻¹ modes involved rather complex collective vibrations of stretching and twisting of the C–C and C–N bonds on the imidazolium ring and the C–H bonds on the propyl chain. The 3073.3 cm⁻¹ and 3076.5 cm⁻¹ peaks mainly involved the stretching modes of the C–H bonds on the methyl group and the propyl chain. The downshifted vibrations at 1636.3 cm⁻¹ and 1634.4 cm⁻¹ mainly came from the stretching of the C=C double bond on the ring that was farther away from the [CuCl₄]²⁻ complex, as shown in Figure 2. Evidently, the shift in vibrational frequencies was caused by the adsorption and interaction of the Cu complex near the imidazolium ring.

In Figure 3, we present (a) the measured C₂H₂ conversion rate X_A and (b) the vinyl chloride monomer (VCM) selectivity S_{VCM} as a function of on-stream reaction time, for the evaluation experiments of the acetylene hydrochlorination reaction using the CuCl₂–[PrMIm]Cl catalyst at different temperatures. Here we used our typical reaction conditions: CuCl₂ concentration = 0.065 mol L⁻¹, C₂H₂ gas hourly space velocity (GHSV) = 370 h⁻¹, and the reactant feed ratio V_{HCl}:V_{C2H2} = 1.2. There was an initial incubation period for the catalyst, and then the conversion rate reached a maximum. The data in Figure 3a indicate that at the reaction temperature of 140 °C, the maximum C₂H₂ conversion rate reached up to 39%, with a VCM selectivity of about 96%. The maximum conversion rate started to decrease at higher and lower temperatures. The maximum C₂H₂ conversion rate and the corresponding VCM selectivity are plotted as a function of temperature in Supplementary Figure S2. From both Figure 3 and Figure S2, we concluded that for a given CuCl₂ concentration and the C₂H₂ GHSV, the best reaction temperature for catalyst CuCl₂–[PrMIm]Cl was about 140 °C. It exhibited high stability; the conversion rate dropped by only 4% after 12 h on stream.

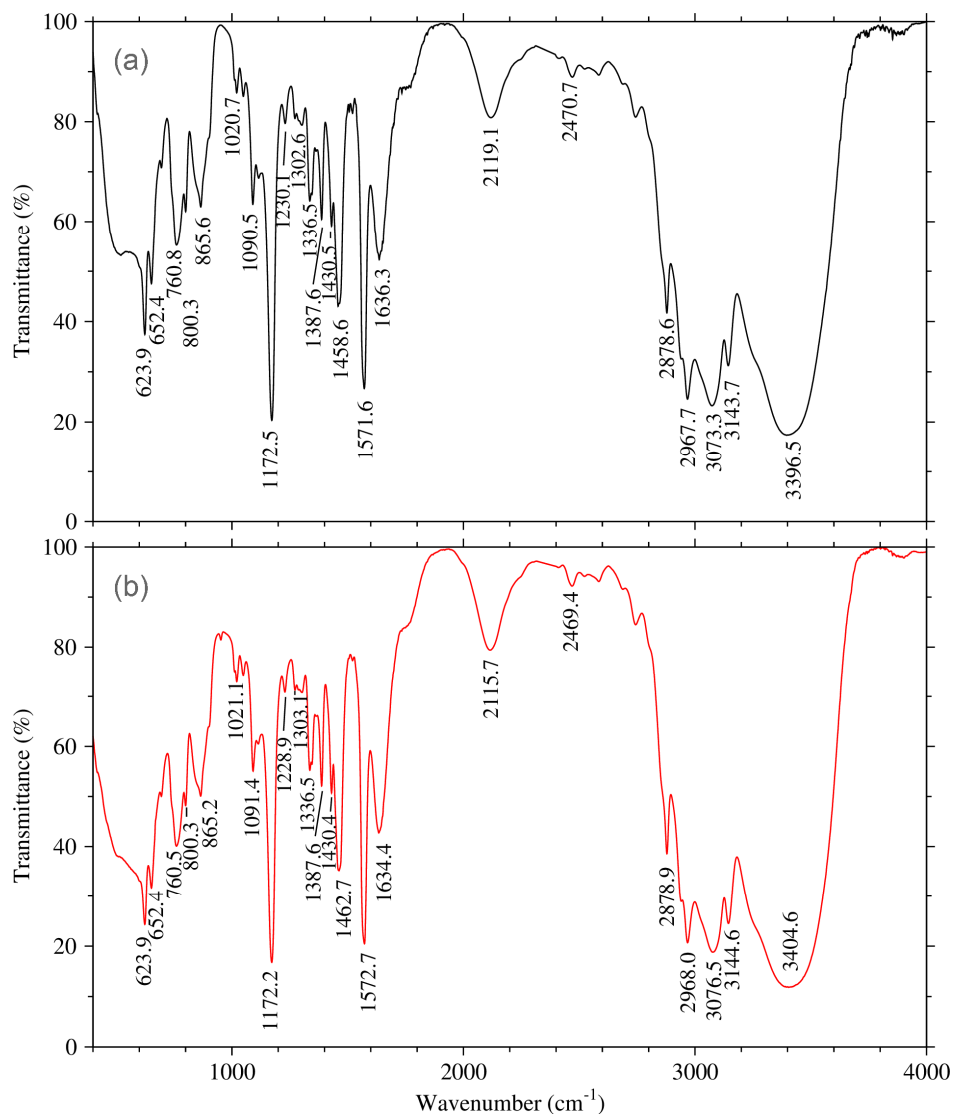


Figure 1. FT-IR spectra of (a) $[\text{PrMIm}] \text{Cl}$ and (b) the catalyst $\text{CuCl}_2\text{-}[\text{PrMIm}] \text{Cl}$.

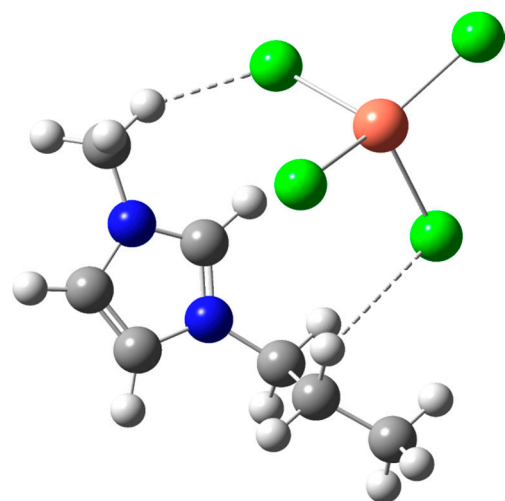


Figure 2. The structure of the $[\text{CuCl}_4]^{2-}$ complex adsorbed on to the cation $[\text{PrMIm}]^+$, as calculated using the computational chemistry software, Gaussian 16. Here the blue, the smallest light grey, dark grey, brick red in the upper right corner, and green balls represent N, H, C, Cu, and Cl atoms, respectively.

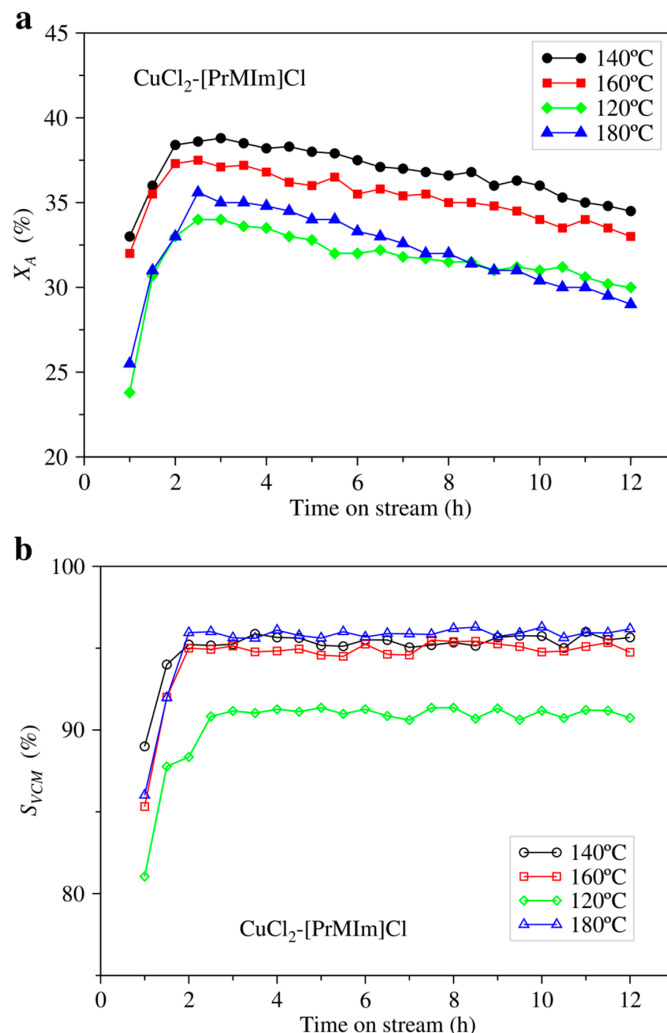


Figure 3. (a) C_2H_2 conversion rate X_A and (b) VCM selectivity S_{VCM} of the catalyst $\text{CuCl}_2\text{-[PrMIm]Cl}$ as a function of reaction time at different temperatures. Reaction conditions: Concentration of $\text{CuCl}_2 = 0.065 \text{ mol}\cdot\text{L}^{-1}$, C_2H_2 GHSV = 370 h^{-1} , feed volume ratio $V_{\text{HCl}}:V_{\text{C}_2\text{H}_2} = 1.2$.

To understand why the initial incubation period was necessary, we did XPS analysis of the fresh $\text{CuCl}_2\text{-[PrMIm]Cl}$ catalyst as prepared before the reaction. The $2p$ core level XPS spectrum of Cu is shown in Figure 4. The spectrum was analyzed using the XPSPeak 4.1 software, and the C 1s core level peak at 284.8 eV was used to calibrate the binding energy, to get rid of possible charge effect. We obtained the binding energy of 932.24 eV for the Cu $2p_{3/2}$ electrons. Comparison with typical data for various valence states of Cu in the XPS handbook [34] indicates that this binding energy is close to that of CuCl and Cu^0 , while the binding energy of CuCl_2 is 935.0 ± 0.5 eV. Among various compounds containing Cu^{2+} , only for CuS and Cu(OAc)_2 , the binding energy of the Cu $2p_{3/2}$ may be compatible to Figure 4. Clearly, they were not present in our samples. Furthermore, a typical Cu^{2+} peak is expected to have strong companion peaks, whereas we only found relatively rather weak companion peaks in the figure at 959.9 eV and 941.6 eV, with a relative signal strength that is consistent with Cu^+ or Cu^0 . Therefore, Figure 4 suggests that CuCl_2 in [PrMIm]Cl was reduced to CuCl . The introduction of HCl could re-oxidize CuCl into CuCl_2 [35]. Indeed, the oxidization capability of HCl on metallic catalytic species in acetylene hydrochlorination have been known for a long time [2,5]. Similar reduction of the cationic catalytic species has been known essentially for all other metal catalysts for acetylene hydrochlorination as well, including the highly active Au/C catalyst. Therefore, it is a common phenomenon that an initial incubation period for the catalytic activity is needed [36]. Hutchings and coworkers proposed that the catalytically active Au^{3+} species could be

reduced to Au^0 by the carbon support during the catalyst preparation process, while other factors also had significant influences [37]. While it is well known that C_2H_2 can reduce the cationic catalytic species and cause loss of catalytic activity [21], we suspect that the IL $[\text{PrMIm}] \text{Cl}$ itself might also become reductive during the catalyst preparation process, in the absence of the oxidative HCl .

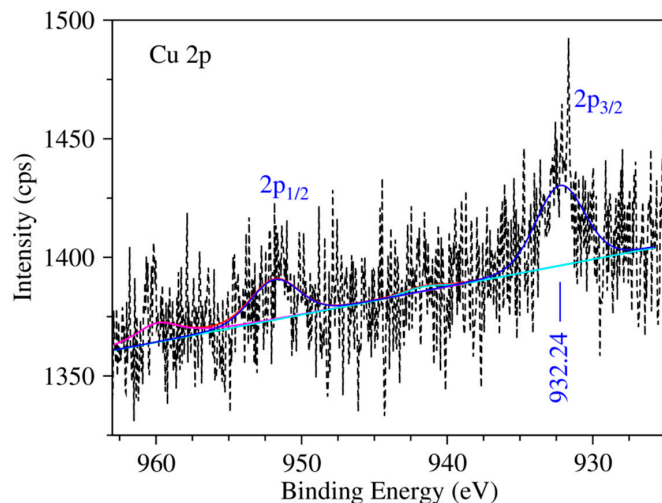


Figure 4. XPS spectrum of Cu 2p core electrons for the fresh as-prepared catalyst $[\text{PrMIm}] \text{Cl}-\text{CuCl}_2$. The binding energy of the observed $2p_{3/2}$ peak is 932.24 eV.

We repeated the above experiment but for other ILs with anion Cl^- . Among these ILs, the $\text{CuCl}_2\text{-}[\text{BMIm}] \text{Cl}$ combination had an optimal reaction temperature of about 160 °C. Nonetheless, the difference between 140 °C and 160 °C was small. We obtained an initial maximum acetylene conversion rate of about 32%. It had a VCM selectivity of about 96%, close to that of the $\text{CuCl}_2\text{-}[\text{PrMIm}] \text{Cl}$ combination. Other $\text{CuCl}_2\text{-IL}$ combinations exhibited relatively lower catalytic activity.

In Table 1, we list the maximum C_2H_2 conversion rate and corresponding VCM selectivity for the CuCl_2 catalyst when different ILs were used as the reaction media. In order to facilitate the comparison, we chose the same reaction conditions including temperature 140 °C and the same C_2H_2 GHSV.

Table 1. Catalytic performance of CuCl_2 , using IL $[\text{M}] \text{Cl}$ with different cations $[\text{M}]^+$ as the reaction media

M	EMIm	PrMIm	BMIm	HMIIm	OMIm	AMIm	HEMIm	BMMIm
X_A (%)	22	39	32	24	15	18	16	12
S_{VCM} (%)	93	96	96	94	90	93	88	85

Reaction conditions: 140 °C, C_2H_2 GHSV = 370 h⁻¹, $V_{\text{HCl}}:V_{\text{C}_2\text{H}_2} = 1.2$, concentration of $\text{CuCl}_2 = 0.065 \text{ mol L}^{-1}$.

Shown in Figure 5 is the bar chart of the data in Table 1. It tells that among all ILs studied, $[\text{PrMIm}] \text{Cl}$ had the highest acetylene conversion rate. In terms of VCM selectivity, the difference between these ILs was not as dramatic. In fact, the main difference between these different ILs lies in the length of the alkyl chains, as one can tell from their structures as listed in Supplementary Table S1. From left to right in Figure 5, namely, from EMIm to OMIm, the names of the cations can be represented uniformly by $C_n\text{MIm}$, with $n = 2, 3, 4, 6, 8$. The allyl group in AMIm contains a C=C double bond, HEMIm contains an extra hydroxyl group $-\text{OH}$, and BMMIm contains an extra methyl group. These detailed structural differences have a strong influence on the adsorption of the Cu complexes and the formation of intermediate transition states, and have thus changed the catalytic activity of the corresponding $\text{CuCl}_2\text{-IL}$ catalysts.

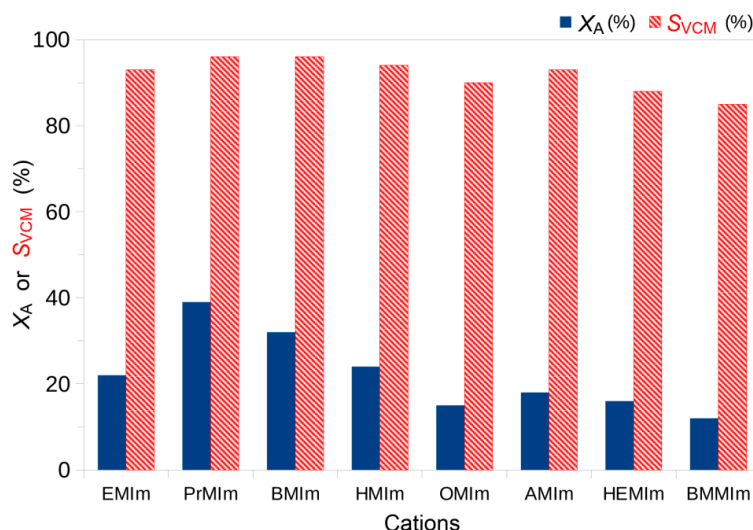


Figure 5. Acetylene conversion rate X_A and VCM selectivity S_{VCM} of the CuCl_2 catalyst, using IL $[\text{M}] \text{Cl}$ with different cations $[\text{M}]^+$ as the reaction media. Reaction temperature $140\text{ }^\circ\text{C}$, C_2H_2 GHSV = 370 h^{-1} , $V_{\text{HCl}}:V_{\text{C}_2\text{H}_2} = 1.2$, and $[\text{CuCl}_2] = 0.065\text{ mol L}^{-1}$.

We also studied the catalytic performance of different metal chlorides as catalysts using the ILs as the reaction media. The result for acetylene conversion rate and the VCM selectivity using $[\text{PrMIm}] \text{Cl}$ as the reaction media is shown in Table 2 and the bar chart of Figure 6. From Table 2 and Figure 6, it is easily seen that except CuCl_2 for which the C_2H_2 conversion rate was nearly 40%, the catalytic activities of all other metal chlorides were low. Overall, the trend for the activity exhibits a positive correlation with the standard electrode potential of the metal ions, in agreement with [1]. We also tried $[\text{PrMIm}] \text{Cl}$ alone as the catalyst, but its activity turned out to be very low.

Table 2. Catalytic performance of different metal chlorides, using $[\text{PrMIm}] \text{Cl}$ as the reaction medium.

MCl_x	CuCl_2	FeCl_3	ZnCl_2	SnCl_2	NiCl_2	BiCl_3
X_A (%)	39	19	16	10	15	9
S_{VCM} (%)	96.5	95	96	94	92	93

Reaction conditions: $140\text{ }^\circ\text{C}$, C_2H_2 GHSV = 370 h^{-1} , $V_{\text{HCl}}:V_{\text{C}_2\text{H}_2} = 1.2$, $[\text{CuCl}_2] = 0.10\text{ mol L}^{-1}$.

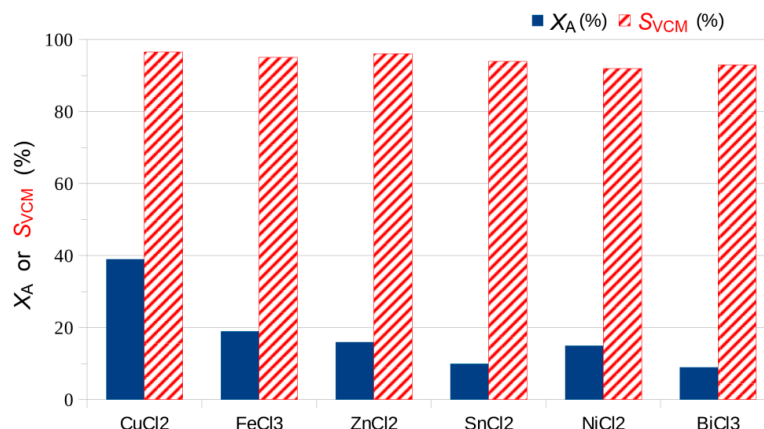


Figure 6. Acetylene conversion rate and VCM selectivity of different metal chlorides, using $[\text{PrMIm}] \text{Cl}$ as the reaction medium. Reaction temperature $140\text{ }^\circ\text{C}$, C_2H_2 GHSV = 370 h^{-1} , $V_{\text{HCl}}:V_{\text{C}_2\text{H}_2} = 1.2$, and concentration of metal chloride 0.10 mol L^{-1} .

Combining Figures 5 and 6, we concluded that the best combination was $\text{CuCl}_2\text{-}[\text{PrMIm}]Cl$. Therefore, we shall focus our study on this combination.

Next, we studied the effect of the concentration of CuCl_2 on the performance of the $\text{CuCl}_2\text{-}[\text{PrMIm}]Cl$ catalyst. Shown in Figure 7 are the conversion rate and selectivity as a function of CuCl_2 concentration. The result reveals that, in a large range of the CuCl_2 concentration, the dependence of the catalytic activity on the CuCl_2 concentration is very weak. It is clear that the conversion was limited by mass transfer as the C_2H_2 conversion rate saturates. In principle, in the very low concentration kinetic regime, the conversion rate should be roughly proportional to the concentration. As the concentration increases, the conversion rate tends to saturate. The data in Figure 7 indicate that the kinetic regime of proportionality was lower than 0.025 mol L^{-1} , which is the lowest concentration studied in the experiment. Indeed, we see a slight increase of the C_2H_2 conversion rate as a function of CuCl_2 concentration.

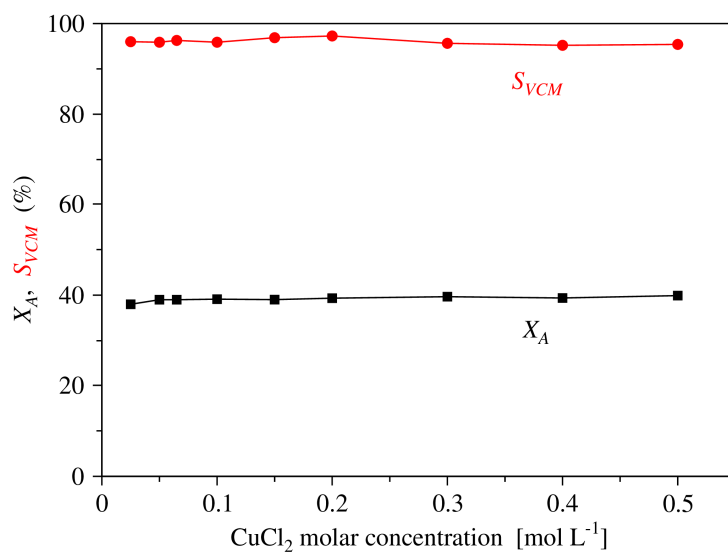


Figure 7. Acetylene conversion rate and VCM selectivity of $\text{CuCl}_2\text{-}[\text{PrMIm}]Cl$, as a function of the concentration of CuCl_2 . Reaction conditions: temperature 140°C , C_2H_2 GHSV = 370 h^{-1} , $V_{\text{HCl}}:V_{\text{C}_2\text{H}_2} = 1.2$.

For comparison, we also performed a control experiment using $[\text{PrMIm}]Cl$ alone as the catalyst, and the result demonstrated that the acetylene conversion rate was negligibly small, as compared to the combination. In addition, we performed a similar reaction using AC supported CuCl_2 as the catalyst, with the same amount of Cu as for the lowest CuCl_2 concentration (0.025 mol L^{-1}) case in Figure 7. After 2 h incubation time, the acetylene conversion rate reached its maximum of 18.5%, under the same reaction conditions. This was substantially lower than the maximum conversion rate, 38%, of the $\text{CuCl}_2\text{-}[\text{PrMIm}]Cl$ catalyst at $[\text{CuCl}_2] = 0.025 \text{ mol L}^{-1}$, which is also close to the maximum rate 39% at $[\text{CuCl}_2] = 0.065 \text{ mol L}^{-1}$. It should be noted, however, due to the presence of the AC support, the experiment with the Cu/AC catalyst cannot be viewed as a good control. Nonetheless, it might be reasonable to assume that, without the AC support, the performance of CuCl_2 alone would be poorer. It should be emphasized, however, that since the kinetic regime is below the lowest CuCl_2 concentration in Figure 7, here we mostly compare the saturation values of the acetylene conversion rate with and without the IL. One should be cautious when comparing the reaction rate on a molar basis.

Then we turned to the effect of the GHSV of the reactant gases. Shown in Figure 8 are the acetylene conversion rate and the VCM selectivity of the $\text{CuCl}_2\text{-}[\text{PrMIm}]Cl$ catalyst as a function of GHSV of C_2H_2 . Our result indicates that the VCM selectivity remained unchanged at the level of about 96% as the GHSV increased. However, the C_2H_2 conversion rate has dropped significantly, from 50% to 40%. As one may expect, this more or less reflects that fact that, for a fixed amount of catalyst, increase in GHSV may cause part of C_2H_2 to be removed from the reaction chamber before it has a chance to

react. Nonetheless, we note that the dependence of the conversion rate on GHSV was not as strong as we had expected.

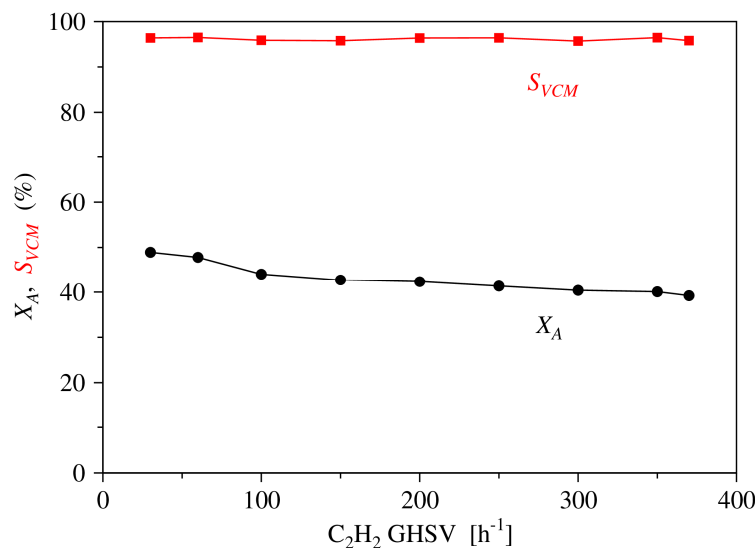


Figure 8. Acetylene conversion rate and VCM selectivity of CuCl₂-[PrMIm]Cl, as a function of C₂H₂ GHSV. Reaction conditions: temperature 140 °C, CuCl₂ concentration 0.065 mol L⁻¹, V_{HCl}:V_{C2H2} = 1.2.

It should be mentioned that the systematic variations of the catalytic activity with various parameters in Figures 3, 7 and 8 indicate that our experimental results are fully reproducible.

2.2. Mechanistic Study Using DFT

Now we present our result from DFT calculations. Unless mentioned explicitly, all calculations were done with DMol3.

First, we calculated the catalytic reaction process assuming [PrMIm]Cl as the catalyst without the participation of CuCl₂. To determine where the most likely adsorption site is located, we calculated the LUMO of the cation [PrMIm]⁺, which is shown in Supplementary Figure S3. It can be seen that, near the two N atoms, there exist the largest unoccupied *p* orbitals, which help to adsorb HCl or C₂H₂ molecules. Therefore, the active adsorption sites are in the neighborhood of the N atoms on the imidazolium ring, as expected.

Then we proceeded to determine the structural relation between the anion Cl⁻ and the cation [PrMIm]⁺ inside the IL. According to [23], Cl⁻ needs to be in the neighborhood of [PrMIm]⁺ and form strong chemical adsorption. Possible structures are shown in Figure 9. The structure in Figure 9b has a slightly lower energy than Figure 9a (by 2.27 kcal/mol), and is thus more stable. However, we emphasize that these are the (meta-)stable structures of a single pair of anion and cation. It does not necessarily mean that the anions and cations in the bulk IL will keep such structures. To determine which case is right for the bulk IL, we calculated the IR spectra for both [PrMIm]⁺ alone and the [PrMIm]-Cl structures shown Figure 9b. The calculated IR spectra are shown in Figure 10. The main difference between these two structures is that there appear to be three very strong vibrational modes for [PrMIm]-Cl at 982.7 cm⁻¹, 2763.3 cm⁻¹ and 3042.7 cm⁻¹. The IR spectrum for the structure in Figure 9a is roughly the same, with the strongest 2763.3 cm⁻¹ peak downshifted to 2759.73 cm⁻¹. The animations of the vibrational modes show that these modes are associated with the strong binding between the anion Cl⁻ and the cation [PrMIm]⁺. The frequencies of other vibrational modes are also modified slightly by Cl⁻. These computed IR spectra are to be compared with those measured experimentally, shown in Figure 1a. We find that these three very strong modes are clearly absent in the measured spectrum, while other modes with relatively lower intensity can be found in the FT-IR data. This suggests that the Cl⁻ anions in the bulk IL are in the unbound state, rather than tightly

adsorbed to any specific cations. This picture is in fact consistent with its ionic liquid nature. Therefore, our further calculations were all based on the cation $[\text{PrMIm}]^+$ without the presence of Cl^- .

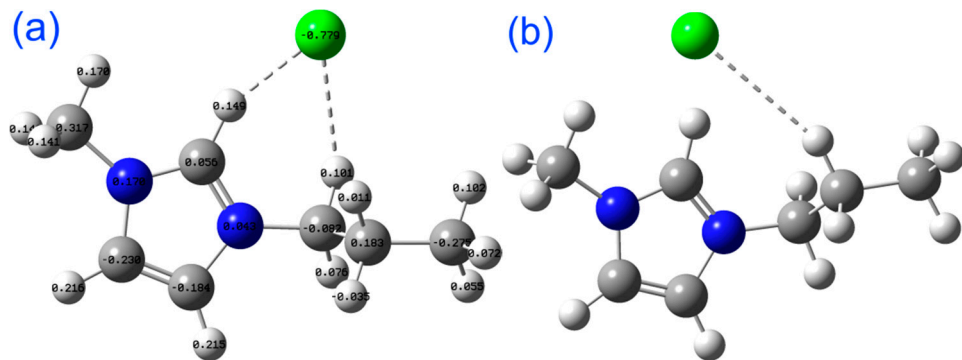


Figure 9. Possible structural relationship between the anion and the cation of the IL $[\text{PrMIm}] \text{Cl}$. (a) A 6-element or (b) 7-element ring forms with the Cl^- anion, C, N, and H atoms. Also labeled in the left panel is the charge distribution. Here the blue, smallest light grey, dark gray, and green balls represent N, H, C, and Cl atoms, respectively. Unlike the imidazolium ring, the 6- and 7-element rings are not as stable, since the dashed lines here only indicate moderately strong Coulomb attractions.

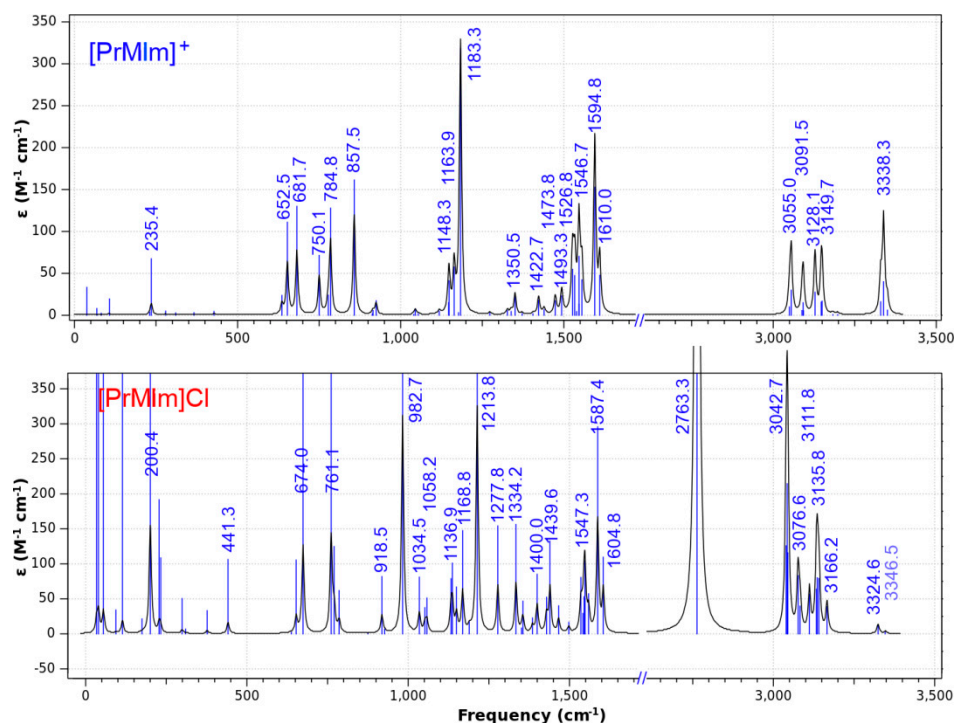


Figure 10. Infrared spectrum of the $[\text{PrMIm}]^+$ cation and the $[\text{PrMIm}]\text{-Cl}$ structure shown in Figure 9b, as calculated via DFT. Very strong vibration modes appear in the lower panel, at 982.7 cm^{-1} , 2763.3 cm^{-1} and 3042.7 cm^{-1} . The animation of the calculated vibrations shows that they are related to the Cl^- anion. Other vibration frequencies have also showed small shift due to the influence of Cl^- .

According to our DFT calculations, the possible reaction path when $[\text{PrMIm}] \text{Cl}$ alone is used as the catalyst is shown in Figure 11, following the direction of the arrows. The adsorption (Ads) of the reactants (R) C_2H_2 on the IL contributes a fairly small decrease to the system energy. This may have to do with the symmetric, non-dipolar charge distribution of C_2H_2 . There is a rather high energy barrier for the intermediate transition state (TS). As the VCM forms, the system energy decreases by the amount of the binding energy, followed by the desorption (Des) of VCM. Finally, one obtains the product (P) VCM. The system energy change is small as well for the Des step, suggesting that the

adsorption of VCM on the IL is also weak. The system energy E and the Gibbs free energy G at each stage are shown in Figure 12, as the red and blue curves, respectively. The data for E and G are listed in Table 3. It can be seen that the barriers for the energy and the Gibbs free energy are as high as 27.28 kcal/mol and 29.57 kcal/mol, respectively. Therefore, the reaction following this path is rather slow. It should be noted that it is the barrier in the Gibbs free energy that determines the reaction rate, even though the energy barrier is often used in the discussion.

It should also be pointed out that, since the reaction takes place in the liquid phase, the free energy should not contain the pV term, namely, we have $G = E - ST$. Both the zero point energy (ZPE) and finite temperature (140°C) corrections are considered in the energy and free energy calculations.

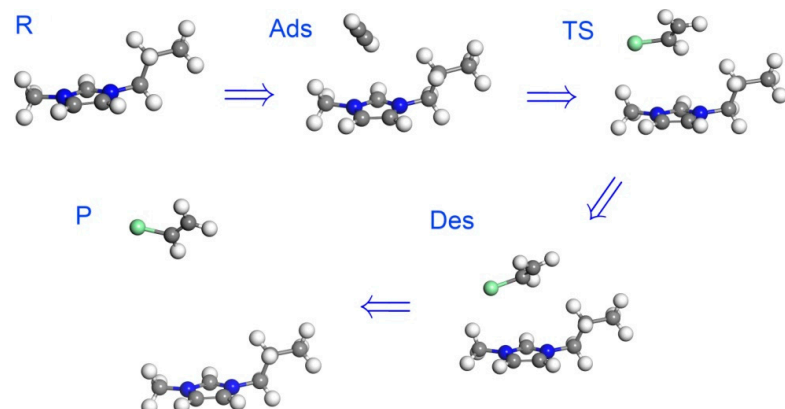


Figure 11. Reaction path of acetylene hydrochlorination, using $[\text{PrMIm}]Cl$ alone as the catalyst. Shown here is a process participated by the $[\text{PrMIm}]^+$ cation. The blue, light grey, dark grey, and green balls represent N, H, C, and Cl atoms, respectively.

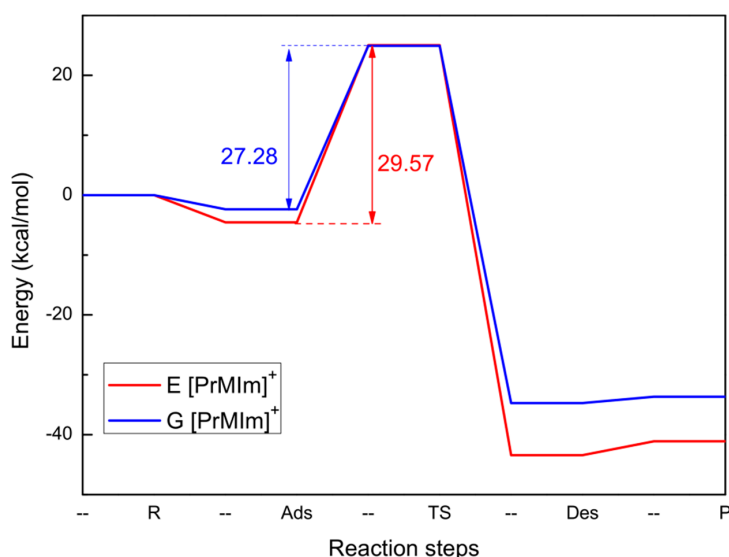


Figure 12. Step-by-step reaction process, in which the reactants C_2H_2 and HCl are adsorbed and react near the active N sites of $[\text{PrMIm}]Cl$. Here $[\text{PrMIm}]^+$ serves as the catalyst. The red and blue lines represent the change in energy E and in the Gibbs free energy G , respectively.

Table 3. Energy levels of the reaction steps shown in Figure 12 (kcal/mol).

Energy	R	Ads	TS	Des	P
$[\text{PrMIm}]^+ : E$	0	-4.54422	25.02324	-43.40721	-41.09202
$[\text{PrMIm}]^+ : G$	0	-2.36146	24.91584	-34.7227	-33.65141

To verify that we have found the right transition state, we did an intrinsic reaction coordinate (IRC) scan. The obtained energy curve is shown in Figure 13 as a function of IRC. The forward evolution leads to the Des state, while the reverse evolution leads back to the Ads state (plus HCl). This confirms that we have indeed found the correct transition state. Figure 13 also shows that the forward reaction has a much lower energy barrier than the backward reaction. This is because acetylene hydrochlorination is an exothermic reaction with a high reaction heat.

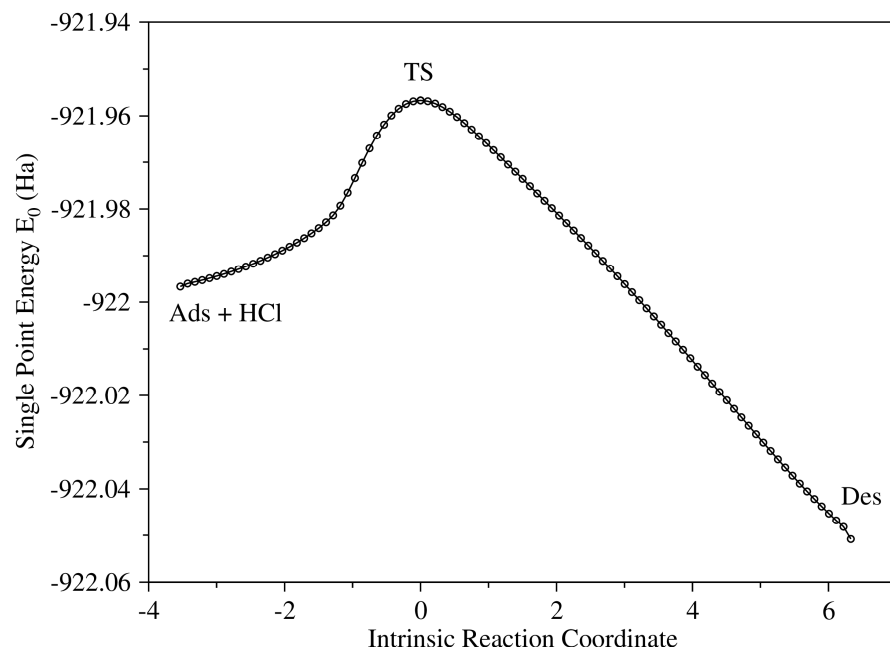


Figure 13. Energy curve from the IRC scan of the TS state in Figure 12, calculated using Gaussian 16. Starting from the saddle point of the TS state, the forward and backward scan lead to the Des and Ads (plus HCl) states, respectively. The forward reaction has a lower energy barrier.

Besides the interaction between the ILs and HCl as well as C_2H_2 , we studied how CuCl_2 participates in the catalysis. It is known that in a Cl^- rich environment, CuCl_2 often exists in the form of $[\text{CuCl}_4]^{2-}$ and $[\text{Cu}_2\text{Cl}_6]^{2-}$. An isolated $[\text{CuCl}_4]^{2-}$ usually has a (meta)stable square planar or flattened tetrahedral structure. Careful studies [38,39] show that the structure of $[\text{CuCl}_4]^{2-}$ exhibits a continuous distribution, with the most probable angle of about 136° between two Cu–Cl bonds. There is also a fairly large probability for this angle to be 90° . The former corresponds to a flattened tetrahedron, while the latter to a planar square. The reason that regular tetrahedron structure is unstable is that there exists very strong Jahn-Teller distortion in this system, which leads to strong structural deformation [39]. Thus far, there is still no consensus about the most probable angle. However, it is certain that due to the existence of all different possible angles, there are structural phase transitions at certain temperatures. Similarly, an isolated $[\text{Cu}_2\text{Cl}_6]^{2-}$ complex may also exist in planar structure or flattened edge-sharing double-tetrahedral structure. In both cases, the planar structure has a higher energy, and is thus a meta-stable state. For example, for $[\text{CuCl}_4]^{2-}$, the energy of the square planar structure is higher than that of flattened tetrahedral structure by 11.60 kcal/mol. Shown in Supplementary Figure S4 are the stable structures of (a) $[\text{CuCl}_4]^{2-}$ and (b) $[\text{Cu}_2\text{Cl}_6]^{2-}$, corresponding to flattened tetrahedral and flattened edge-sharing double tetrahedral structures, respectively.

Next, we calculated the catalytic reactions near the Cu(II) site of the CuCl_2 catalyst. In the $[\text{PrMIm}]\text{Cl}$ reaction media, since CuCl_2 appears in the form of $[\text{CuCl}_4]^{2-}$ and $[\text{Cu}_2\text{Cl}_6]^{2-}$, they will be attracted to the neighborhood of the N atoms of the cationic $[\text{PrMIm}]^+$ complex.

The reaction steps and the energy levels for each step are shown in Figure 14. The red (E) and blue (G) lines represent the energy and Gibbs free energy as catalyzed by $[\text{Cu}_2\text{Cl}_6]^{2-}$, while the black

(E) and green (G) lines are for the energy and Gibbs free energy levels as catalyzed by $[\text{CuCl}_4]^{2-}$. All E and G levels with respect to the reactants are also listed in Table 4.

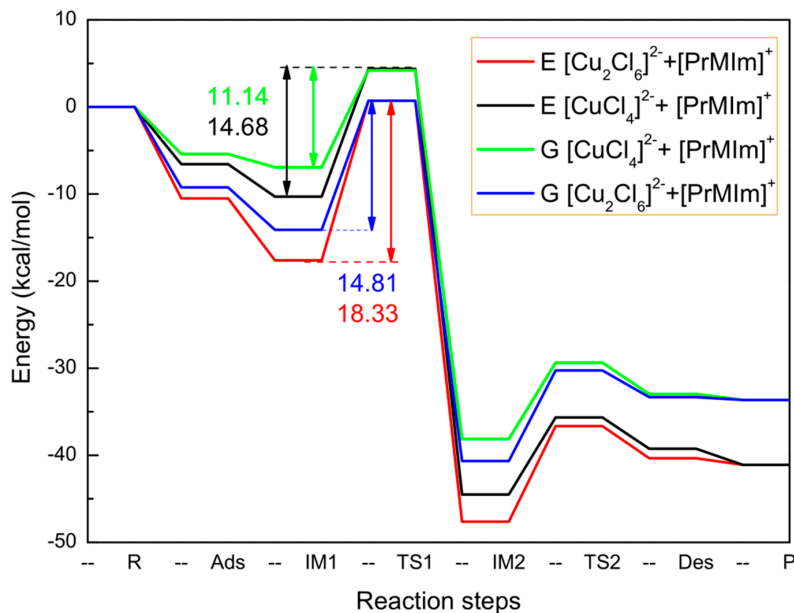


Figure 14. Step-by-step reaction process, in which the reactants C_2H_2 and HCl are adsorbed and react near the Cu(II) active site. The red and blue lines represent the cases with the participation of $[\text{Cu}_2\text{Cl}_6]^{2-}$ while the black and green lines represent the cases catalyzed by $[\text{CuCl}_4]^{2-}$.

Table 4. Energy levels of the reaction steps shown in Figure 14 (kcal/mol).

Energy	R	Ads	IM1	TS1	IM2	TS2	Des	P
$[\text{Cu}_2\text{Cl}_6]^{2-}$: E	0	-10.4962	-17.6158	-0.7144	-47.6207	-36.6548	-40.3414	-41.0920
$[\text{Cu}_2\text{Cl}_6]^{2-}$: G	0	-9.2365	-14.1023	-0.7096	-40.6574	-30.2568	-33.3256	-33.6514
$[\text{CuCl}_4]^{2-}$: E	0	-6.5772	-10.3016	4.3732	-44.4982	-35.6521	-39.2439	-41.0920
$[\text{CuCl}_4]^{2-}$: G	0	-5.4169	-46.9216	4.2157	-38.1267	-29.3651	-32.9651	-33.6514

Now there are two intermediate states and two transition states. For the case of $[\text{Cu}_2\text{Cl}_6]^{2-}$, the structures of each step are shown in Figure 15. As can be seen from the Figure, $[\text{Cu}_2\text{Cl}_6]^{2-}$ is adsorbed to the neighborhood of the N atoms of $[\text{PrMIm}]\text{Cl}$. Then a C_2H_2 molecule is adsorbed to $[\text{Cu}_2\text{Cl}_6]^{2-}$ (Ads), with an adsorption energy of -10.50 kcal/mol. Next, C_2H_2 and $[\text{Cu}_2\text{Cl}_6]^{2-}$ react and form an intermediate state IM1, for which the C atoms of C_2H_2 replace two of the Cl atoms of $[\text{Cu}_2\text{Cl}_6]^{2-}$, and the two Cl atoms form covalent bonds with the C atoms. The energy of IM1 is lower than the reactant by 17.62 kcal/mol. After the transition state TS1 (with energy 0.71 kcal/mol), one of the two Cu–C bonds and one of the two C–Cl valence bonds break apart, and the detached Cl atom forms a covalent bond with Cu, and thus the intermediate state IM2. The IM2 state has the lowest energy in the entire reaction path, -47.6206 kcal/mol. Then the system passes through the transition state TS2, and the other Cu–C bond breaks apart, while an HCl molecule comes to the neighborhood. The HCl molecule combines with the broken $\text{C}_2\text{H}_2\text{Cl}$, contributes an H atom, and forms $\text{C}_2\text{H}_3\text{Cl}$, while the leftover Cl atom joins the Cu_2Cl_5 complex, and recovers Cu_2Cl_6 . In this Des stage, the system energy is -40.34 kcal/mol, relative to the reactants. The two transition states have fairly high energy barriers. Especially for TS1, the breaking of the Cu–C bond leaves two free atoms such that the system energy is substantially higher than that of IM1, by 18.33 kcal/mol. Note that the energy of the Des stage is slightly higher than the product. The energy barrier from IM1 to TS1 is substantially higher than that from IM2 to TS2, and therefore is the determining step for the reaction rate. If one considers Gibbs free energy, then the energy levels will differ slightly, and the reaction barrier would become 14.81 kcal/mol.

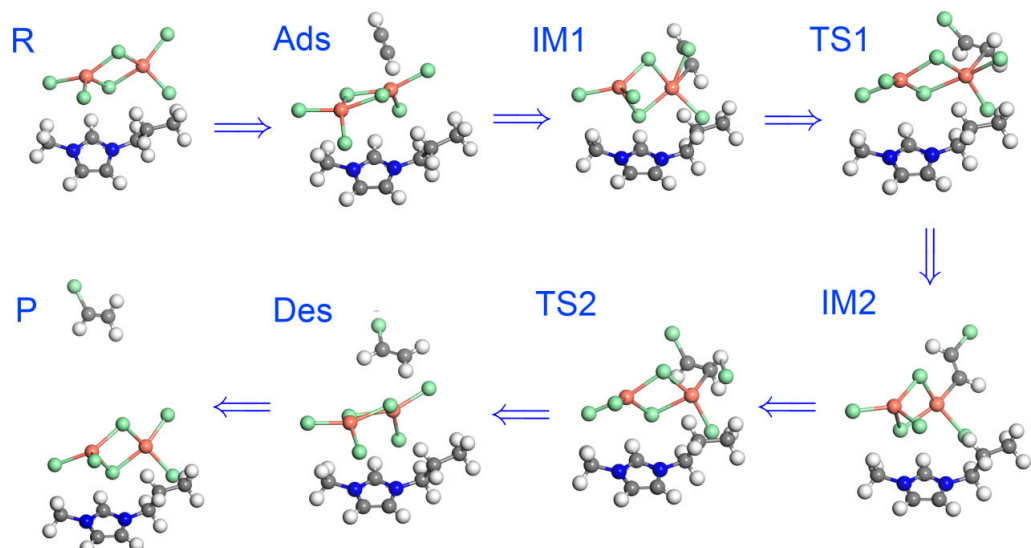


Figure 15. Reaction path of acetylene hydrochlorination near the Cu(II) atom, as catalyzed jointly by the catalyst CuCl_2 and the reaction media $[\text{PrMIm}]\text{Cl}$. Shown is the process in which the anion $[\text{Cu}_2\text{Cl}_6]^{2-}$ participates in the catalysis. Here Cu exists in the form of $[\text{Cu}_2\text{Cl}_6]^{2-}$, and is adsorbed near the N atoms of $[\text{PrMIm}]\text{Cl}$. Here, brick red spheres denote Cu atoms, and the color coding for other atoms is the same as Figure 11.

The molecular structures of each reaction step for the case of $[\text{CuCl}_4]^{2-}$ are shown in Figure 16. The process is very similar to the case of $[\text{Cu}_2\text{Cl}_6]^{2-}$ above. First, the $[\text{CuCl}_4]^{2-}$ complex is adsorbed to the N atoms of $[\text{PrMIm}]\text{Cl}$, followed by adsorption of a C_2H_2 molecule to $[\text{CuCl}_4]^{2-}$ (Ads), with an adsorption energy of -6.58 kcal/mol . Then C_2H_2 reacts with $[\text{CuCl}_4]^{2-}$ and form the intermediate state IM1, for which the C atoms of C_2H_2 replace two Cl atoms of $[\text{CuCl}_4]^{2-}$ and form two covalent Cu-C bonds, and these two Cl atoms now form covalent C-Cl bonds with the C atoms of C_2H_2 . IM1 has an energy of -10.30 kcal/mol . Next, via the transition state TS1, one of the Cu-C bonds and one of the C-Cl bonds break apart, and form a Cu-Cl bond, and thus an intermediate state IM2, which has the lowest energy of the entire reaction path, -44.50 kcal/mol . Now via the transition state TS2, the other Cu-C bond breaks apart, while an HCl molecule approaches. The H atom of HCl detaches and combines with the $\text{C}_2\text{H}_2\text{Cl}$ complex, yielding $\text{C}_2\text{H}_3\text{Cl}$, while the Cl atom groups with CuCl_3 and recovers CuCl_4 . In the Des step, various covalent bonds relax to their equilibrium lengths so that stable $\text{C}_2\text{H}_3\text{Cl}$ appears, with a system energy of -39.24 kcal/mol . The two transition states have rather high energy barriers. In particular, after the Cu-C bond breaks, the TS1 state has a dramatically elevated energy level with respect to IM1. The barrier from IM1 to TS1 is 16.67 kcal/mol , higher than that from IM2 to TS2, and thus is the decisive step for the reaction rate. Taking into account of the entropy at 140°C , the reaction barrier in terms of Gibbs free energy is reduced down to 11.14 kcal/mol , implying that high temperature makes the forward reaction easier.

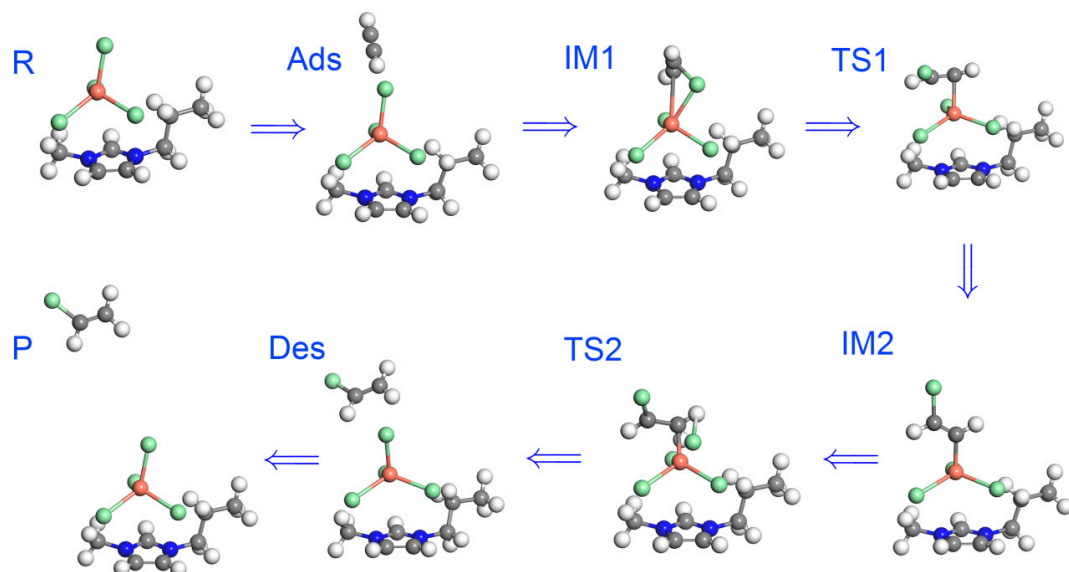


Figure 16. Reaction path of acetylene hydrochlorination near the Cu(II) atom, as catalyzed jointly by the catalyst CuCl_2 and the reaction media $[\text{PrMIm}]\text{Cl}$. Shown is the process in which the anion $[\text{CuCl}_4]^{2-}$ participates in the catalysis. Here Cu exists in the form of $[\text{CuCl}_4]^{2-}$, and is adsorbed near the N atoms of $[\text{PrMIm}]\text{Cl}$. The color coding is the same as Figure 15.

For the two forms of Cu(II) complexes, $[\text{PrMIm}]\text{Cl}$ not only provides Cl^- , but also participates in the adsorption of the reactants so that it acts synergistically with CuCl_2 in the catalysis. As can be seen from Figures 15 and 16, the shape of $[\text{PrMIm}]^+$ deviates significantly from its free form due to attractions from the reactants and the Cu complexes. Nonetheless, we do not consider $[\text{PrMIm}]\text{Cl}$ as an active catalytic ingredient in Figures 15 and 16, as the catalytic reactions mainly take place near the Cu complexes.

Comparing the catalytic reaction processes under the two forms of Cu complexes, one can see that the $[\text{CuCl}_4]^{2-}$ case has an overall lower energy. Furthermore, the rate determining Gibbs free energy barrier, 11.14 kcal/mol, is significantly lower than that for the $[\text{Cu}_2\text{Cl}_6]^{2-}$ case, 14.81 kcal/mol. Therefore, one can conclude that, when using $[\text{PrMIm}]\text{Cl}$ as the reaction media, the largest contribution of CuCl_2 to the catalytic reaction comes from the form of $[\text{CuCl}_4]^{2-}$. Nonetheless, the contribution in the form of $[\text{Cu}_2\text{Cl}_6]^{2-}$ is not completely negligible, as the energy barrier difference between them is not huge (about $\Delta G = 4.5 \text{ k}_{\text{B}}T$). On the other hand, Figures 12 and 14 represent catalytic reactions using $[\text{PrMIm}]\text{Cl}$ and CuCl_2 as the catalyst, respectively. From the height of the barriers, one concludes that the contribution from $[\text{PrMIm}]\text{Cl}$ as a catalyst to the acetylene hydrochlorination reaction rate is negligible, since the reaction rate R has an exponential dependence on the barrier height ΔG , namely,

$$R \propto T e^{-\Delta G/k_{\text{B}}T}. \quad (1)$$

For $T = 413 \text{ K}$, we have $k_{\text{B}}T/\text{molecule} = 0.8207 \text{ kcal/mol}$. Based on this relationship, the contribution from $[\text{Cu}_2\text{Cl}_6]^{2-}$ is about 1.14% of that of $[\text{CuCl}_4]^{2-}$, while the contribution of $[\text{PrMIm}]\text{Cl}$ as a catalyst, with the barrier $\Delta G = 27.28 \text{ kcal/mol}$, is 2.88×10^{-9} times that of $[\text{CuCl}_4]^{2-}$, which is completely negligible.

In summary, our DFT calculations show that the main catalysis takes place near the Cu(II) active site. In the environment of IL, Cu(II) often exists in the form of $[\text{CuCl}_4]^{2-}$ and $[\text{Cu}_2\text{Cl}_6]^{2-}$ complexes, and are adsorbed to the cation of the IL. At the same time, the IL facilitates the reaction by attracting C_2H_2 and HCl to the neighborhood of the Cu complex. While both Cu complexes can catalyze the acetylene hydrochlorination reaction, $[\text{CuCl}_4]^{2-}$ dominates the contribution. Without CuCl_2 , the IL alone exhibits very low catalytic activity, as is consistent with our experiment.

3. Discussion

Our experimental result for the activity of the CuCl_2 -IL catalysts should be compared to that in the literature. We notice that Cao et al. [19] obtained a C_2H_2 conversion rate of 68% at a relatively low GHSV for the catalyst CuCl_2 -[BMIm]Cl, whereas we obtained the best conversion rate of about 39% for CuCl_2 -[PrMIm]Cl but at a much higher GHSV = 370 h^{-1} . For CuCl_2 -[BMIm]Cl, our best conversion rate at this high GHSV was about 32%. However, they also reported a fairly rapid drop of the conversion rate with increasing GHSV, while we saw a fairly slow change with GHSV. As indicated in their Figure 6, the conversion rate for different temperatures and CuCl_2 concentrations dropped to about 37–40% when the GHSV was increased to 90 h^{-1} . It seems that if their GHSV had increased further, their conversion rate would have dropped more rapidly to a level below our present result.

Cao's group also studied the effect of different anions on the catalytic activity [23], and found that among ILs with the same cation, catalysts prepared with the one with the anion Cl^- had the best catalytic performance. This was also confirmed by our preliminary result. Nevertheless, as mentioned earlier, we avoided using ILs with non- Cl^- anions altogether since they would inevitably introduce unwanted by-products, such as $\text{C}_2\text{H}_3\text{Br}$, etc.

Our calculated reaction process and reaction mechanism should also be compared with existing literature. The theoretical calculations of Ren et al. showed that under room temperature, the hydrogen bond between C_2H_2 and the ILs is critical in the solubility of C_2H_2 in the ILs [40]. The cations of the ILs may interact strongly with C_2H_2 via $\pi-\pi$ bonding. The length of the alkyl chains does not strongly affect this $\pi-\pi$ bonding. The high solubility helps C_2H_2 to approach the catalyst more closely so as to facilitate the catalytic reaction. Our results of the synergistic effect of the ILs are consistent with the calculated high solubility of C_2H_2 in the ILs.

Regarding the reaction mechanism of [BMIm]Cl alone as the catalyst, [23] did quantitative computations. They thought that at room temperature, the following dynamical balances exist



and they proposed a reaction mechanism. From their results, the formation and opening of hydrogen bond is the key to the catalytic reaction. First of all, the Cl^- anion forms a hydrogen bond with the C(2)-H group on the imidazolium ring so that a six element ring forms, with 1 Cl, 1 N, 2 C, and 2 H atoms. This ring is relatively small in that the C_2H_2 molecule cannot interact strongly with it. When a HCl molecule joins, it may form a $[\text{HCl}_2]^-$ radical with the previous Cl^- , so that the six-element ring is enlarged to be an eight-element ring. In result, the hydrogen bond between the previous Cl^- and the C(2)-H group is weakened while the ring grows, so that a C_2H_2 molecule may be inserted to form an intermediate state. In particular, the C_2H_2 may form a hydrogen bond with the $[\text{HCl}_2]^-$ radical, while it interacts with the imidazolium ring via $\pi-\pi$ bonding. After charge transfer and bond reorganization, a vinyl chloride molecule is formed.

Our calculated process with [PrMIm]Cl as the catalyst should be compared with their proposed mechanism. However, we find that in our case of [PrMIm]Cl, only the six-element ring was involved, and our transition state was confirmed to connect the Ads step with the Des step via an IRC scan, as shown in Figure 13. Nonetheless, we do acknowledge that there might be other reaction paths, connecting the reactants with the products. Indeed, this can be seen from the fact that, for a molecular structure as complicated as [PrMIm]Cl- CuCl_2 , there are multiple meta-stable adsorption structures with slightly different adsorption energies.

Regarding the reactions catalyzed by either $[\text{CuCl}_4]^{2-}$ or $[\text{Cu}_2\text{Cl}_6]^{2-}$, the intermediate IM1 state involves formation of two Cu-C bonds, one of which has to be broken later. This IM1 state has a rather low energy, which is thus expected to have a fairly long lifetime. We could not identify a process

that bypasses the IM1 step and evolves from the Ads step to IM2 directly via the transition state TS1. Should such a process exist, the reaction energy barrier would become very low, and the reaction would become superfast.

Thus far, we are not aware of theoretical calculations about the CuCl₂-IL catalysts for acetylene hydrochlorination that can be compared to our current study. Our calculations show that, without CuCl₂, the reaction rate is essentially negligible. This is different from the findings of [23], but consistent with our own experimental result. The C₂H₂ conversion rate for the regular CuCl₂/AC catalyst from our control experiment under our reaction conditions was 18.5%, much lower than our current result. These results serve as a manifestation of the synergistic effect of CuCl₂ and [PrMIm]Cl in catalyzing the reaction of acetylene hydrochlorination. Microscopically, the Cl⁻ rich environment of the IL leads to the formation of anionic [CuCl₄]²⁻ and [Cu₂Cl₆]²⁻ complexes, which are attracted to the cations of the IL. At the same time, the high solubility of C₂H₂ (as well as HCl) in the IL greatly increases the chances for the reactants as well as the Cu(II) complexes to get close to each other and complete the reaction cycles.

It should be mentioned that the IL calculated in [23] was [BMIm]Cl, rather than [PrMIm]Cl. However, due to the relatively lower catalytic activity of the [BMIm]Cl-CuCl₂ combination, we did not do calculations for the case where [BMIm]Cl acts as the catalyst alone. The different choices of ILs might provide reconciliation between our findings and [23] regarding the catalytic activity of the IL as a catalyst for acetylene hydrochlorination.

For the future, we look to include more metal chlorides and other compounds in our calculations, and have more thorough comparisons between experiment and theory, in hopes to find better metal-IL combinations for which the metal-IL synergy works to yield an excellent catalyst for acetylene hydrochlorination.

4. Materials and Methods

Major imidazolium type of ILs (purity > 99%) include [BMIm]Cl, [BMIm]Br, [PrMIm]Cl, [PrMIm]Br, [EMIm]Cl, [HMIm]Cl, [BMIm]BF₄, [EMIm]BF₄, [BMIm]PF₆, and [EMIm]PF₆, etc., which differ mainly in the length of the alkyl chains and the anions. They were purchased from Lanzhou Greenchem ILS, LICP, CAS. (Lanzhou, China), and used as received. To avoid complications in the VCM selectivity, only ILs with Cl⁻ anions were used. The chemical formulae, molecular weights, and structures of the ILs with Cl⁻ and different alkyl chains can be found in Supplementary Table S1. The metal chlorides were purchased from Alladin Regents (Shanghai) Co. Ltd. High purity reactants C₂H₂ (>99.9%) and HCl (>99.9%) were purchased from Hangzhou Jingong Special Gases, Ltd. and Shanghai Chengkung Gas Industry, Ltd., and used without further purification.

Our gas-liquid phase reaction apparatus for acetylene hydrochlorination is schematically shown in Supplementary Figure S5. To remove residue impurity gases including water and air, the temperature of the reaction chamber was raised gradually to 120 °C and N₂ was let into the reaction path for 20 min. Then we turned on the HCl flow, with a flow rate of 0.5 L/h, to activate the catalyst for 1 h. Next, the temperature of the reaction chamber was raised to the reaction condition, 140 °C, and we turned on the flow of C₂H₂, with a volume feed ratio of V_{HCl}:V_{C2H2} = 1.2. The flow rate was controlled by the mass flow controller (MFC). Before entering the reaction chamber, C₂H₂ was passed through the K₂Cr₂O₇ and H₂SO₄ bottles to remove impurity gas components. The typical GHSV for C₂H₂ was set to be 370 h⁻¹. The temperature of reaction chamber was controlled by the oil bath, whose temperature was measured by the thermal couple (TC). After reaction, the product and residual reactant gases passed through the absorbing bottle, to remove HCl, before they enter the gas chromatography analyzer.

The ILs were pre-processed before the experiments began: we took 15 ml IL in a small glass container, and placed in an oven at 80 °C for 20 min, so that it melted into liquid completely. Then we added the metal chloride MCl_x that had been dried to remove water. After stirring actively in an ultrasonic bath for 10 min, we obtained a homogeneous liquid of IL with MCl_x dissolved. In Supplementary Figure S6, we show the IL [PrMIm]Cl in (a) solid and (b) liquid states and (c) as

a solution of CuCl_2 , exhibiting sand-yellow, light yellow, and green colors, respectively. Then the catalyst was put in the reaction chamber that was placed in an oil bath, as shown in Figure S5.

In order to determine the appropriate reaction temperature, we surveyed the thermodynamic transition temperatures and the thermal decomposition temperature T_d , as shown in Table 5. Here listed are the melting temperature T_m , freezing temperature T_f , glass transition temperature T_g , and T_d . Due to the big size mismatch between the cation and the anion in an IL, and that the cations are normally very large, most ILs exhibit glassy behavior; there are no sharp transition temperatures, unlike that of a good crystalline solid, and the melting and freezing temperatures often differ. For this reason, we find different temperatures from different sources. Nevertheless, except for [BMMIm]Cl, the rest ILs have a T_m below 100 °C. Note that the freezing temperature may be substantially lower than the melting point, implying that the ILs may exhibit supercritical behavior; a melted IL will not freeze until a much lower temperature. For [PrMIm]Cl, one can melt it at 80 °C, then it will remain a liquid at room temperature. More importantly, these ILs are thermally stable above about 250 °C, well above our chosen reaction temperature, 140 °C. On the other hand, we notice that the actual onset temperature for thermal decomposition is substantially lower than T_d , therefore, to maintain long term stability, we chose a reaction temperature that was substantially below T_d as well. At our reaction temperature, the ILs remained in perfect stable liquid state.

Table 5. Thermodynamic transition temperatures of common imidazolium-based ILs and those used in the experiment.

IL	T_m (°C)	T_f (°C)	T_g (°C)	T_d (°C)
[BMIm]Cl	41 ~ 70	-	-76 ~ -69	254
[PrMIm]Cl	60, 62	-140	-	281 ~ 282
[EMIm]Cl	77 ~ 90	73	-	281 ~ 285
[HMIm]Cl	-85, -75	-	-75	253
[OMIm]Cl	12, 12.3	-	-87 ~ -77	243
[AMIm]Cl	17, 49–51	-	-	273
[HEMIm]Cl	60.8 ± 2, 86	-111	-	-
[BMMIm]Cl	79, 99, 100	-	-	-

Note: The melting temperatures were mainly from the ChemSpider website at <http://www.chemspider.com>, and the handbook of ionic liquids [41–43].

The best reaction temperature differs for different ILs. We prepared a series of catalysts of different CuCl_2 –IL combinations, and carried out the evaluation experiment under different parameters, including temperature, CuCl_2 concentration, GHSV of C_2H_2 , and on-stream reaction time, etc. We measured the conversion rate of C_2H_2 , selectivity of VCM, and stability of the catalyst, etc., in order to determine the best IL. In comparison, we also performed control studies with CuCl_2 and ILs alone as separate catalysts, to ascertain the promotional effect of the ILs to CuCl_2 . For CuCl_2 without an IL, we used AC as the support.

Methods of DFT Calculations

Our DFT calculations were performed mainly using the quantum chemistry computation software package DMol3 [44], including the optimization of the molecular structures and the computation of the transitional states. The generalized gradient approximation (GGA) with the Perdew–Burke–Ernzerhof (PBE) functional [45] and all-electron double numerical basis set with polarized function (DNP) have been employed [46]. The convergence tolerance of energy, maximum force and maximum displacement are 1.0×10^{-5} Ha, 2.0×10^{-3} Ha/Å and 5.0×10^{-3} Å (1Ha = 27.21 eV, equivalent to 627.5095 kcal/mol) for geometry optimization. The complete LST/QST search protocol, the SCF tolerance of 1.0×10^{-6} Ha and smearing of 0.005 Ha are set for transition states. The Grimme method for DFT-D correction is considered for all calculations. Each atom in the storage models is allowed to relax to the minimum in the enthalpy without any constraints.

In addition, we also use Gaussian 16 [47] to do independent calculations for some simple molecular optimization and reactions. We employed the widely used B3LYP functional [48–51] with the 6-31G(D) basis set [52,53], which includes the diffusive function corrections and has been known to give reliable results. To ensure better accuracy [54], we chose the unrestricted method for the B3LYP calculations. We use the ‘tight convergence criteria’ set by the software, namely, maximum force 1.5×10^{-5} Ha/Å, root-mean-square (RMS) force 1.0×10^{-5} Ha/Å, maximum displacement 6.0×10^{-5} Å, and RMS displacement 4.0×10^{-5} Å. In addition, we use quadratically convergent self-consistent field algorithm (QC SCF) or XQC SCF to speed up the convergence. The errors for our energy calculations are usually $(0.01\sim 1.0) \times 10^{-5}$ Ha.

5. Conclusions

We have studied the catalytic performance of CuCl_2 among other metal chlorides as a catalyst for gas–liquid phase reactions of acetylene hydrochlorination, using ILs as the reaction media. Among various imidazolium-based ILs with different alkyl chains, we find that when $[\text{PrMIm}]\text{Cl}$ was the reaction media, the metal catalyst exhibited the highest catalytic activity. Under the conditions $T = 140^\circ\text{C}$, C_2H_2 GHSV = 370 h^{-1} , and reactant gas feed volume ratio $V_{\text{HCl}}:V_{\text{C}_2\text{H}_2} = 1.2$, the $[\text{PrMIm}]\text{Cl}-\text{CuCl}_2$ combination exhibits the highest acetylene conversion rate, up to 39%, much higher than the sum of that of the CuCl_2/AC catalyst and of the IL alone as the catalyst. Our DFT calculation of the reaction process for the $[\text{PrMIm}]\text{Cl}-\text{CuCl}_2$ catalyst show that CuCl_2 are adsorbed in the neighborhood of the N atoms of $[\text{PrMIm}]\text{Cl}$, and the main catalytic reactions occur at the Cu(II) active sites. Without the participation of Cu^{2+} , reactions at the N sites of the ILs have a rather high energy barrier and thus this contribution is negligible to the total reaction rate. As for the reactions near the Cu(II) active sites, among the two most common ionic complexes, $[\text{CuCl}_4]^{2-}$ and $[\text{Cu}_2\text{Cl}_6]^{2-}$, the former has the lowest energy barrier, and hence the highest reaction rate. Since the difference in barrier height is not very big, the contribution of the latter is small but should not be simply neglected.

Our result revealed strong synergistic effects between Cu and the ILs in the catalytic reaction of acetylene hydrochlorination. In an IL which contains Cl^- , it is easy for CuCl_2 to attract extra Cl^- to form stable $[\text{CuCl}_4]^{2-}$ and $[\text{Cu}_2\text{Cl}_6]^{2-}$ complexes, which are easily adsorbed to the cation, especially the N atoms of the IL. At the same time, C_2H_2 has a high solubility in the imidazolium type of ILs. This helps to bring C_2H_2 and HCl close to each other and to the Cu(II) complexes. On the other hand, the Cl^- anion of HCl and that of CuCl_2 as well as the Cl^- of the ILs are identical quantum particles. This facilitates the formation of intermediate states and transition states, so as to lower the reaction barrier and expedite the reaction of HCl and C_2H_2 near the Cu(II) sites to form $\text{C}_2\text{H}_3\text{Cl}$.

Supplementary Materials: The following are available online at <http://www.mdpi.com/2073-4344/9/6/504/s1>. Figure S1: TGA curves of the IL $[\text{PrMIm}]\text{Cl}$ (black thick line) and $[\text{BMIm}]\text{Cl}$ (red thin line), Figure S2: The highest C_2H_2 conversion rate X_A and the VCM selectivity S_{VCM} as a function of reaction temperature T , for the catalyst $\text{CuCl}_2\text{-}[\text{PrMIm}]\text{Cl}$. Reaction conditions: CuCl_2 concentration = 0.065 mol L^{-1} , C_2H_2 GHSV = 370 h^{-1} , feed volume ratio $V_{\text{HCl}}:V_{\text{C}_2\text{H}_2} = 1.2$, Figure S3: (a) LUMO orbital and (b) chemical structure of the $[\text{PrMIm}]^+$ cation, as calculated using Gaussian 16. Here the dark gray, light gray and blue balls represent the C, H and Cl atoms, respectively. And the red and green colors represent (different signs of) the LUMO orbitals, Figure S4: Main structure for CuCl_2 to appear in the IL $[\text{Prmim}]\text{Cl}$. Panel (a) is the flattened tetrahedron for the anionic $[\text{CuCl}_4]^{2-}$ complex, and panel (b) is the edge-sharing double tetrahedron structure for the anionic $[\text{Cu}_2\text{Cl}_6]^{2-}$ complex, Figure S5: Schematic diagram of the apparatus for gas–liquid phase reactions using ILs as the solvent and reaction media. After passing through the MFC, C_2H_2 and HCl enter the reaction chamber, which is placed in an oil bath. The residual reactant and product gases then pass through the absorbing bottle, Figure S6: Physical appearance of (a) solid and (b) liquid $[\text{PrMIm}]\text{Cl}$ and (c) its solution of CuCl_2 (placed in a glass, bird view), exhibiting colors of sand-yellow, light yellow, and green, respectively, Table S1: Structures and molecular weights of some common imidazolium-based ILs that were used in the experiments.

Author Contributions: Conceptualization, Y.Y. (Yi Yu), J.Z., and X.L.; Methodology, Y.Y. (Yi Yu) and B.W.; Validation, J.Z. and X.L.; Formal analysis, Y.Y. (Yi Yu); Computation, Y.Y. (Yi Yu); Data curation, Y.Y. (Yi Yu), Y.Y. (Yuxue Yue), B.W., and H.H.; Writing—original draft preparation, Y.Y. (Yi Yu); Writing—review and editing, Y.Y. (Yi Yu), J.Z., and X.L.; Supervision, X.L.; Project administration, J.Z.; Funding acquisition, X.L.

Funding: This work was supported by the National Natural Science Foundation of China (NSFC; grant nos. 21606199 and 21476207) and the Science and Technology Department of Zhejiang Province, China (Projects for Applications of Technology, grant no. 2017C37004).

Conflicts of Interest: The authors declare no conflict of interest.

References

1. Hutchings, G.J. Vapor phase hydrochlorination of acetylene: Correlation of catalytic activity of supported metal chloride catalysts. *J. Catal.* **1985**, *96*, 292–295. [[CrossRef](#)]
2. Johnston, P.; Carthey, N.; Hutchings, G.J. Discovery, Development, and Commercialization of Gold Catalysts for Acetylene Hydrochlorination. *J. Am. Chem. Soc.* **2015**, *137*, 14548–14557. [[CrossRef](#)] [[PubMed](#)]
3. Malta, G.; Freakley, S.J.; Kondrata, S.A.; Hutchings, G.J. Acetylene hydrochlorination using Au/carbon: a journey towards single site catalysis. *Chem. Commun.* **2017**, *53*, 11733–11746. [[CrossRef](#)] [[PubMed](#)]
4. Xu, H.; Luo, G.H. Green production of PVC from laboratory to industrialization: State-of-the-art review of heterogeneous non-mercury catalysts for acetylene hydrochlorination. *J. Ind. Eng. Chem.* **2018**, *65*, 13–25. [[CrossRef](#)]
5. Nkosi, B.; Coville, N.J.; Hutchings, G.J. Vapour phase hydrochlorination of acetylene with group VIII and IB metal chloride catalysts. *Appl. Catal.* **1988**, *43*, 33–39. [[CrossRef](#)]
6. Wieiaut, J.P.; Vandalfsen, J. Undefined. *Rec. Truv. Chim.* **1932**, *51*, 636.
7. Wang, S.J.; Shen, B.X.; Song, Q.L. Kinetics of acetylene hydrochlorination over bimetallic Au–Cu/C catalyst. *Catal. Lett.* **2010**, *134*, 102–109. [[CrossRef](#)]
8. Wang, L.; Shen, B.X.; Zhao, J.G.; Bi, X.T. Trimetallic Au–Cu–K/AC for acetylene hydrochlorination. *Can. J. Chem. Eng.* **2017**, *95*, 1069–1075. [[CrossRef](#)]
9. Zhang, H.Y.; Dai, B.; Wang, X.G.; Xu, L.L.; Zhu, M.Y. Hydrochlorination of acetylene to vinyl chloride monomer over bimetallic Au–La/SAC catalysts. *J. Ind. Eng. Chem.* **2012**, *18*, 49–54. [[CrossRef](#)]
10. Zhang, H.Y.; Li, W.; Jin, Y.H.; Sheng, W.; Hu, M.C.; Wang, X.Q.; Zhang, J.L. Ru–Co(III)–Cu(II)/SAC catalyst for acetylene hydrochlorination. *Appl. Catal. B Environ.* **2016**, *189*, 56–64. [[CrossRef](#)]
11. Zhao, J.; Xu, J.T.; Xu, J.H.; Ni, J.; Zhang, T.T.; Xu, X.L.; Li, X.N. Activated-carbon-supported Gold–Cesium(I) as highly effective catalysts for hydrochlorination of acetylene to vinyl chloride. *ChemPlusChem* **2015**, *80*, 196–201. [[CrossRef](#)]
12. Zhao, J.; Zhang, T.T.; Di, X.X.; Xu, J.T.; Gu, S.C.; Zhang, Q.F.; Ni, J.; Li, X.N. Activated carbon supported ternary Gold–Cesium(I)–Indium(III) catalyst for the hydrochlorination of acetylene. *Catal. Sci. Technol.* **2015**, *5*, 4973–4984. [[CrossRef](#)]
13. Zhai, Y.Y.; Zhao, J.; Di, X.X.; Di, S.X.; Wang, B.L.; Yue, Y.X.; Sheng, G.F.; Lai, H.X.; Guo, L.L.; Wang, H.; et al. Carbon-supported perovskite-like CsCuCl₃ nanoparticles: a highly active and cost-effective heterogeneous catalyst for the hydrochlorination of acetylene to vinyl chloride. *Catal. Sci. Technol.* **2018**, *8*, 2901–2908. [[CrossRef](#)]
14. Zhao, J.; Gu, S.C.; Xu, X.L.; Zhang, T.T.; Di, X.X.; Pan, Z.Y.; Li, X.N. Promotional effect of copper(II) on an activated carbon supported low content bimetallic Gold–Cesium(I) catalyst in acetylene hydrochlorination. *RSC Adv.* **2015**, *5*, 101427–101436. [[CrossRef](#)]
15. Wang, B.L.; Lai, H.X.; Yue, Y.X.; Sheng, G.F.; Deng, Y.Q.; He, H.H.; Guo, L.L.; Zhao, J.; Li, X.N. Zeolite supported ionic liquid catalysts for the hydrochlorination of acetylene. *Catalysts* **2018**, *8*, 351. [[CrossRef](#)]
16. Welton, T. Room temperature ionic liquids: Solvents for synthesis and catalysis. *Chem. Rev.* **1999**, *99*, 2071–2084. [[CrossRef](#)]
17. Wasserscheid, P.; Welton, T. *Ionic Liquids in Synthesis*; Wiley-VCH Verlag: Stuttgart, Germany, 2002.
18. Vekariya, R.L. A review of ionic liquids: Applications towards catalytic organic transformations. *J. Mol. Liq.* **2017**, *227*, 44–60. [[CrossRef](#)]
19. Qin, G.; Song, Y.H.; Jin, R.; Shi, J.; Yu, Z.Y.; Cao, S.K. Gas–liquid acetylene hydrochlorination under nonmercuric catalysis using ionic liquids as reaction media. *Green Chem.* **2011**, *13*, 1495–1498. [[CrossRef](#)]
20. Zhao, J.; Gu, S.C.; Xu, X.L.; Zhang, T.T.; Yu, Y.; Di, X.X.; Ni, J.; Pan, Z.Y.; Li, X.N. Supported ionic-liquid-phase-stabilized Au(III) catalyst for acetylene hydrochlorination. *Catal. Sci. Technol.* **2016**, *6*, 3263–3270. [[CrossRef](#)]

21. Zhao, J.; Yu, Y.; Xu, X.L.; Di, S.X.; Wang, B.L.; Xu, H.; Ni, J.; Guo, L.L.; Pan, Z.Y.; Li, X.N. Stabilizing Au(III) in supported-ionic-liquid-phase (SILP) catalyst using CuCl₂ via a redox mechanism. *Appl. Catal. B* **2017**, *206*, 175–183. [CrossRef]
22. Li, Y.; Dong, Y.Z.; Li, W.; Han, Y.; Zhang, J.L. Improvement of imidazolium-based ionic liquids on the activity of ruthenium catalyst for acetylene hydrochlorination. *Mol. Catal.* **2017**, *443*, 220–227. [CrossRef]
23. Zhou, X.F.; Xu, S.G.; Liu, Y.L.; Cao, S.K. Mechanistic study on metal-free acetylene hydrochlorination catalyzed by imidazolium-based ionic liquids. *Mol. Catal.* **2018**, *461*, 73–79. [CrossRef]
24. Zhao, J.; Yue, Y.X.; Sheng, G.F.; Wang, B.L.; Lai, H.X.; Di, S.X.; Zhai, Y.Y.; Guo, L.L.; Li, X.N. Supported ionic liquid-palladium catalyst for the highly effective hydrochlorination of acetylene. *Chem. Eng. J.* **2019**, *360*, 38–46. [CrossRef]
25. Xu, J.H.; Zhao, J.; Xu, J.T.; Zhang, T.T.; Li, X.N.; Di, X.X.; Ni, J.; Wang, J.G.; Cen, J. Influence of surface chemistry of activated carbon on the activity of gold/activated carbon catalyst in acetylene hydrochlorination. *Ind. Eng. Chem. Res.* **2014**, *53*, 14272–14281. [CrossRef]
26. Zhao, J.; Zhang, T.T.; Di, X.X.; Xu, J.T.; Xu, J.H.; Feng, F.; Ni, J.; Li, X.N. Nitrogen-modified activated carbon supported bimetallic Gold–Cesium(I) as highly active and stable catalyst for the hydrochlorination of acetylene. *RSC Adv.* **2015**, *5*, 6925–6931. [CrossRef]
27. Zhao, J.; Xu, J.T.; Xu, J.H.; Zhang, T.T.; Di, X.X.; Ni, J.; Li, X.N. Enhancement of Au/AC acetylene hydrochlorination catalyst activity and stability via nitrogen-modified activated carbon support. *Chem. Eng. J.* **2015**, *262*, 1152–1160. [CrossRef]
28. He, H.H.; Zhao, J.; Wang, B.L.; Yue, Y.X.; Sheng, G.F.; Wang, Q.T.; Yu, L.; Hu, Z.-T.; Li, X.N. Highly active AuCu-based catalysts for acetylene hydrochlorination prepared using organic aqua regia. *Materials* **2019**, *12*, 1310. [CrossRef]
29. Di, X.X.; Zhao, J.; Yu, Y.; Xu, X.L.; Gu, S.C.; He, H.H.; Zhang, T.T.; Li, X.N. One-pot synthesis of nitrogen and sulfur co-doped activated carbon supported AuCl₃ as efficient catalysts for acetylene hydrochlorination. *Chin. Chem. Lett.* **2016**, *27*, 1567–1571. [CrossRef]
30. Zhao, J.; Wang, B.L.; Yue, Y.X.; Sheng, G.F.; Lai, H.X.; Wang, S.S.; Yu, L.; Zhang, Q.F.; Feng, F.; Hu, Z.T.; et al. Nitrogen- and phosphorus-codoped carbon-based catalyst for acetylene hydrochlorination. *J. Catal.* **2019**, *373*, 240–249. [CrossRef]
31. Zhao, J.; Wang, B.L.; Xu, X.L.; Yu, Y.; Di, S.X.; Xu, H.; Zhai, Y.Y.; He, H.H.; Guo, L.L.; Pan, Z.Y.; et al. Alternative solvent to aqua regia to activate Au/AC catalysts for the hydrochlorination of acetylene. *J. Catal.* **2017**, *350*, 149–158. [CrossRef]
32. Zhao, J.; Wang, B.L.; Yue, Y.X.; Di, S.X.; Zhai, Y.Y.; He, H.H.; Sheng, G.F.; Lai, H.X.; Zhu, Y.H.; Guo, L.L.; et al. Towards a greener approach for the preparation of highly active Gold/Carbon catalyst for the hydrochlorination of ethyne. *J. Catal.* **2018**, *365*, 153–162. [CrossRef]
33. Nakamoto, K. *Infrared and Raman Spectra of Inorganic and Coordination Compounds, Part B: Applications in Coordination, Organometallic, and Bioinorganic Chemistry*, 6th ed.; Wiley: Hoboken, NJ, USA, 2009.
34. Moulder, J.F.; Stickle, W.F.; Sobol, P.E.; Bomben, K.D. *Handbook of X-ray Photoelectron Spectroscopy*; Chastain, J., King, R.C., Jr., Eds.; Physical Electronics Inc.: Eden Prairie, MN, USA, 1995.
35. Greenwood, N.N.; Earnshaw, A. *Chemistry of the Elements*, 2nd ed.; Butterworth-Heinemann: Oxford, UK, 1997.
36. Malta, G.; Kondrat, S.A.; Freakley, S.J.; Davies, C.J.; Dawson, S.; Liu, X.; Lu, L.; Dymkowski, K.; Fernandez-Alonso, F.; Mukhopadhyay, S.; et al. Deactivation of a single-site Gold-on-Carbon acetylene hydrochlorination catalyst: An X-ray absorption and inelastic neutron scattering study. *ACS Catal.* **2018**, *8*, 8493–8505. [CrossRef]
37. Conte, M.; Davies, C.J.; Morgan, D.J.; Carley, A.F.; Johnston, P.; Hutchings, G.J. Characterization of Au³⁺ species in Au/C catalysts for the hydrochlorination reaction of acetylene. *Catal. Lett.* **2014**, *144*, 1–8. [CrossRef]
38. Rakitin, Y.V.; Kalinnikova, V.T.; Khodasevichb, S.G.; Novotortsev, V.M. Structures of the complex ions [CuCl₄]²⁻ and [CuCl₅]³⁻. *Russ. J. Coord. Chem.* **2007**, *33*, 891–895. [CrossRef]
39. Kelley, A.; Nalla, S.; Bond, M.R. The square-planar to flattened-tetrahedral CuX₄²⁻ (X = Cl, Br) structural phase transition in 1,2,6-trimethylpyridinium salts. *Acta Cryst.* **2015**, *B71*, 48–60. [CrossRef]
40. Zhao, X.; Xing, H.; Yang, Q.; Li, R.; Su, B.; Bao, Z.; Yang, Y.; Ren, Q. Differential solubility of ethylene and acetylene in room-temperature ionic liquids: A theoretical study. *J. Phys. Chem. B* **2012**, *116*, 3944–3953. [CrossRef]
41. Zhang, S.J.; Lu, X.M.; Zhou, Q.; Li, X.H.; Zhang, X.P.; Li, S.C. *Ionic Liquids: Physicochemical Properties*; Elsevier: Amsterdam, The Netherlands, 2009.

42. Haynes, W.M.; Lide, D.R.; Bruno, T.J. CRC Handbook of Chemistry and Physics, 97th ed.; CRC Press, Taylor & Francis Group: Boca Raton, FL, USA, 2017.
43. Plechkova, N.V.; Seddon, K.R. Ionic liquids completely UnCOILED—Critical expert overviews; Wiley: Hoboken, NJ, USA, 2015.
44. Delley, B. From molecules to solids with the DMol3 approach. *J. Chem. Phys.* **2000**, *113*, 7756–7764. [[CrossRef](#)]
45. Perdew, J.P.; Burke, K.; Ernzerhof, M. Generalized gradient approximation made simple. *Phys. Rev. Lett.* **1996**, *77*, 3865–3868. [[CrossRef](#)] [[PubMed](#)]
46. Delley, B. An all-electron numerical method for solving the local density functional for polyatomic molecules. *J. Chem. Phys.* **1990**, *92*, 508–517. [[CrossRef](#)]
47. Frisch, M.J. Gaussian 16, Revision A.03; Gaussian, Inc.: Wallingford, CT, USA, 2016.
48. Becke, A.D. Density-functional thermochemistry. III. The role of exact exchange. *Chem. Phys.* **1993**, *98*, 5648–5652. [[CrossRef](#)]
49. Lee, C.; Yang, W.T.; Parr, R.G. Development of the Colle–Salvetti correlation-energy formula into a functional of the electron density. *Phys. Rev. B* **1988**, *37*, 785. [[CrossRef](#)]
50. Stephens, P.J.; Devlin, F.J.; Chabalowski, C.F.; Frisch, M.J. Ab Initio calculation of vibrational absorption and circular dichroism spectra using density functional force fields: A comparison of local, nonlocal, and hybrid density functional. *J. Phys. Chem.* **1994**, *98*, 11623–11627. [[CrossRef](#)]
51. Kim, K.; Jordan, K.D. Comparison of density functional and MP2 calculations on the water monomer and dimer. *J. Phys. Chem.* **1994**, *98*, 10089–10094. [[CrossRef](#)]
52. Hehre, W.J.; Ditchfield, R.; Pople, J.A. Self-consistent molecular orbital methods. XII. Further extensions of Gaussian-type basis sets for use in molecular-orbital studies of organic-molecules. *Chem. Phys.* **1972**, *56*, 2257–2261. [[CrossRef](#)]
53. Hariharan, P.C.; Pople, J.A. Accuracy of AH equilibrium geometries by single determinant molecular-orbital theory. *Mol. Phys.* **1974**, *27*, 209–214. [[CrossRef](#)]
54. Foresman, J.B.; Frisch, A. Exploring Chemistry with Electronic Structure Methods, 2nd ed.; Gaussian, Inc.: Pittsburgh, PA, USA, 1996.



© 2019 by the authors. Licensee MDPI, Basel, Switzerland. This article is an open access article distributed under the terms and conditions of the Creative Commons Attribution (CC BY) license (<http://creativecommons.org/licenses/by/4.0/>).